Applied Catalysis B: Environmental 97 (2010) 57–71

Contents lists available at ScienceDirect

Applied Catalysis B: Environmental

journal homepage: www.elsevier.com/locate/apcatb

Metal–support interactions in Pt/Al_2O_3 and Pd/Al_2O_3 catalysts for CO oxidation

A.S. Ivanova[a], E.M. Slavinskaya[a], R.V. Gulyaev[a], V.I. Zaikovskii[a], O.A. Stonkus[b], I.G. Danilova[a], L.M. Plyasova[a], I.A. Polukhina[a], A.I. Boronin[a,b,*]

[a] Boreskov Institute of Catalysis SB RAS, Pr. Lavrentieva, 5, 630090 Novosibirsk, Russia
[b] Novosibirsk State University, Pirogova 2, 630090 Novosibirsk, Russia

ARTICLE INFO

Article history:
Received 11 January 2010
Received in revised form 15 March 2010
Accepted 19 March 2010
Available online 27 March 2010

Keywords:
Supported catalysts
Alumina
Palladium
Platinum
CO oxidation
SMSI
HRTEM
XPS
TPR-H_2
Catalysis

ABSTRACT

Platinum and palladium catalysts supported on γ-Al_2O_3 were studied by XRD, UV–vis DRS, HRTEM, TPR-H_2, XPS together with measurements of their catalytic properties. The properties of the catalysts denoted as Pt(Pd)/Al_2O_3(*X*)-*Y* (*X—the calcination temperature of support*, °C; *Y—the calcination temperature of catalyst*, °C) were studied as a function of the temperatures used for calcination of the support and/or the catalyst in oxygen or in a reaction mixture of CO + O_2. It was found that the deposition of Pt or Pd on γ-Al_2O_3 did not alter the structure of the support. Two types of the Pt and Pd particles were typically present on the γ-Al_2O_3 surface: individual particles with dimensions of 1.5–3 nm and agglomerates about 100 nm in size. In the catalysts calcined at relatively low temperatures (Pt/Al_2O_3(550)-450), platinum was present in the form of metal clusters. However, in the Pd/Al_2O_3(550)-450 catalyst, the palladium particles were almost completely decorated with a thin layer of an aluminate phase. These structures are not reduced in hydrogen in the temperature range of −15 to 450 °C, and are stable to treatment in a reaction mixture of CO + O_2. Pd deposition on the γ-Al_2O_3-800 support was found to result in stabilization of the active component in two main forms, Pd^0 and PdO, with varying degrees of interaction due to the decoration effect. Calcination at the low temperature of 550 °C led to the formation of a so-called "core–shell structure", where a palladium metal core is covered with a thin shell of an aluminate phase. Depending on the calcination temperature of the catalyst in the range of 450–1000 °C, the morphological form of the active component was converted from the "core-shell" state to a state consisting of two phases, Pd^0 and PdO, with a gradual decrease of the Pd^0/PdO ratio, weakening the interaction with the support and the growth of palladium particles. Under the action of the reaction mixture, the Pd/Al_2O_3(800)-(450,600,800,1000) catalysts underwent changes in the Pd^0/PdO ratio, which regulates the light-off temperature. After catalyst calcination at the highest temperature used in this study, 1200 °C, the palladium particles became much larger due to the loss of the palladium interaction with the support. Only the metal phase of palladium was observed in these catalysts, and their catalytic activity decreases substantially.

1. Introduction

Aluminum oxide is widely used as a support for various catalysts, mostly in the form of γ-Al_2O_3 [1]. According to Morterra and Magnacca [2], this is due to a number of factors. First, the alumina surface has Lewis acid sites, which have a major effect on the distribution and state of the active components and catalytic activity in different reactions. Second, alumina is characterized by high thermal stability [3]. Third, the support effect on the catalyst performance has been widely investigated, and it has been clarified that acidic support materials enhance the electron-deficiency of noble metals more than basic supports [4,5]. Fourth, γ-Al_2O_3 has a defective spinel structure containing a certain fraction of cation vacancies ($Al_8[Al_{13(1/3)}\square_{2(2/3)}]O_{32}$) [6], facilitating interaction of the active component with the support. Also, it is well known [7–10] that the redox properties of supported noble metals are largely determined by the interactions with their support. For example, according to literature data, the noble metal in Pd(Pt)/γ-Al_2O_3 can exist in at least two different states. Using XPS [9] and Raman spectroscopy [10], Otto et al. showed that palladium existed in two different states on the surface of Pd/γ-Al_2O_3 samples. PdO was observed at Pd concentrations exceeding 0.5 wt.% according to binding energy values. At Pd concentrations below 0.5 wt.%, the binding energy was shifted by 1.6 eV to higher values in comparison with bulk PdO due to the formation of a finely dispersed oxide product of the interaction between palladium and alumina [9]. Similar results were obtained by Gigola and coworkers [11,12] for Pd/γ-Al_2O_3 samples with low palladium concentrations. The relative contributions of these phases depend on the precursor con-

* Corresponding author at: Boreskov Institute of Catalysis SB RAS, Pr. Lavrentieva, 5, 630090 Novosibirsk, Russia. Tel.: +7 383 326 95 37; fax: +7 383 330 80 56.
E-mail address: boronin@catalysis.ru (A.I. Boronin).

0926-3373/$ – see front matter © 2010 Elsevier B.V. All rights reserved.
doi:10.1016/j.apcatb.2010.03.024

centration, with a higher degree of interaction being obtained at low concentrations. Similar results were also obtained for the Pt/γ-Al_2O_3 system [9,13]. At low concentrations, the metal exists in a finely dispersed cluster form, with sizes lower than 2 nm, whereas large particles resembling Pt black are formed at higher concentrations.

In other studies [14,15], it has been demonstrated that an Al_2O_3 support affects the temperature shift of the Pd–PdO phase transformation and its temperature hysteresis for nanosized palladium. It has also been shown that the support has a significant effect on the phase transformation, most likely due to the effects of the interaction between the metal (or metal oxide) and support. The effects of the reaction medium on the palladium redox processes occurring during methane oxidation have also been analyzed [15].

Despite all of the results reported in the literature, the nature of the metal–support interaction in Pd/γ-Al_2O_3 and Pt/γ-Al_2O_3 catalysts is still not well understood. Several possible structures have been suggested for the Pd interaction with the Al_2O_3 surface. They include the formation of a two-dimensional surface complex [16], the formation of a palladium–aluminate phase due to stabilization of the active cations in the vacant octahedral sites of the support according to EXAFS data [17] and palladium stabilization in the form of PdO_2 and deficiently coordinated Pd^{2+} [9]. In the Pt/Al_2O_3 system, the interaction between Pt and Al_2O_3 can result from PtO_2 dissolution in the surface Al_2O_3 layers or the formation of a $PtO_2{\cdot}Al_2O_3$ complex [13]. Nevertheless, until now the nature of the interaction between the active component and the support in Pd/γ-Al_2O_3 and Pt/γ-Al_2O_3 systems and the effect of the CO + O_2 reaction mixture or oxidative treatment at various temperatures on this interaction have not been studied in detail by physicochemical and catalytic methods.

The first step in the preparation of many heterogeneous catalysts is impregnation. In this process, metal complexes dissolved in an aqueous solution contact with a porous oxide catalyst supports such as alumina. During a contact time of typically 1 h, the noble metal adsorbs from the aqueous solution on the high surface area support. Consequently, the type of noble metal precursor substantially affects its adsorption. H_2PtCl_6 [18,19], $Pd(NO_3)_2$ [20] and $Pd(CH_3COO)_2$ [21] are the noble metal compounds most widely used for support impregnation. Therefore, it seemed desirable to compare the properties of Pd/γ-Al_2O_3 and Pt/γ-Al_2O_3 catalysts prepared using similar precursors—Pt and Pd nitrates.

Second important step of the catalyst preparation is the application of the oxidative and/or reductive treatments in oxygen or hydrogen ambient. One of the main reasons of the research interest to oxidative treatments of Pd, Pt containing catalysts is tightly bound with the application of pollution control devices, such as catalytic converters, where the oxidation of exhaust gases including carbon monoxide takes place. Palladium, platinum and alumina are one of the main components of the catalysts used for the gas neutralization. In these converters the reduction by H_2 treatment is not provided for the preliminary stage of the catalyst preparation. Therefore, it was important to investigate the interaction of palladium with alumina in the course of standard procedure of the catalyst calcination. It is noteworthy that temperature in converters varies in a wide range determining the peculiarities of Pd–alumina system. Thus, it appeared to be sufficient reasons for the systematic study of the support and catalyst oxidative treatment in a wide temperature range of 450–1200 °C.

Another reason of interest to the announced problem is the result of investigations performed in [22,23] where it was shown that palladium can redisperse or sinter under the oxidative treatments. The effect of Pd particles spreading was observed in an oxidizing atmosphere. Besides it was proposed the formation of the interface layer between palladium and support. Also, it is necessary to note that at subsequent works devoted to investigation of Pd/Al_2O_3 catalysts, the oxidative treatments were usually used as standard procedures [24–27].

Thus, one of the aims of the presented work was to study the influence of oxidative treatments at different temperatures on the state, morphology and interaction of palladium and platinum with γ-alumina.

The oxidation of CO on alumina-supported noble metal catalysts is known to take place via a single-site competitive Langmuir–Hinshelwood mechanism [28]. It should be noted that the states of the metal and oxidized forms of the active component are important for CO oxidation by oxygen on platinum metal. The relative concentrations of these forms and mutual reversible phase transformations play a substantial role in effects such as the hysteresis and self-oscillation phenomena and reaching the active reaction regime [29]. In this respect, the effect of the support on the formation of the strong interaction, as well as on the dispersion and phase of the active component, largely determines the specifics of the oxidation reaction in comparison with the same reaction on bulk metals (single and polycrystals, metal blacks, etc.).

In the current study, we systemized the states of palladium and platinum using a wide range of supports and catalyst oxidative treatment temperatures. We observed for the first time the specific interaction of palladium with aluminum oxide, which can be characterized as the formation of "core–shell" structures known in other systems. The metal and oxide phase states of the active components on the aluminum oxide surfaces were spectrally and morphologically characterized. The conditions of their existence and efficiency in CO oxidation were also determined.

2. Experimental

2.1. Catalysts

The Al_2O_3 supports were synthesized by precipitation from an aluminum nitrate solution with aqueous NH_4HCO_3 (ρ = 1.05–1.06 g/cm^3) at definite pH values and temperatures, followed by filtration and washing of the precipitate with distilled water until there were no nitrates in the filtrate. The synthesized samples were dried in air at room temperature and in a drying oven at 110 °C for 2–14 h, followed by calcination in a dry air flow at 550 or 800 °C for 4 h.

Supported Pt and Pd catalysts were prepared by incipient wetness impregnation of the supports with aqueous platinum (palladium) nitrate solution followed by drying and calcination at 450–1200 °C for 4 h.

The catalysts are denoted as Pt(Pd)/Al_2O_3(*X*)-*Y*. Here *X* and *Y* denote the calcination temperatures (°C) of the support and the catalyst, respectively, e.g., Pt(Pd)/Al_2O_3(550)-450. The Pt(Pd) concentration in the samples was equal to 1.03(1.02) wt.%.

2.2. Methods of investigation

Atomic absorption spectrometry was used for determination of the concentrations of the main components to an accuracy of 0.01–0.03% [30].

X-ray diffraction (XRD) studies were carried out using a D-500 (Siemens, Germany) diffractometer with CuK_α (λ = 1.5418 Å) monochromatic radiation. The diffraction profiles were recorded both in a continuous mode and in a step-by-step scanning mode at 0.05–0.1° 2θ steps with a dwell time of 20–30 s depending on the sample crystallinity. The phases were identified by comparison of the measured set of the interfacial distances d_i and the corresponding intensities of the diffraction maximums I_i with those found in the JCPDS database (PCPDF Win. Ver 1.30, JCPDS ICDD, Swarthmore, PA, USA, 1997).

High-resolution transmission electron microscope (HRTEM) images were obtained using a JEM-2010 electron microscope (JEOL, Japan) with a lattice-fringe resolution of 0.14 nm at an accelerating voltage of 200 kV. The high-resolution images of periodic structures were analyzed by the Fourier method. Local energy-dispersive X-ray analysis (EDXA) was carried out using an EDX spectrometer (EDAX Co.) fitted with a Si (Li) detector with a resolution of 130 eV. The samples for the HRTEM study were prepared on perforated carbon film mounted on a copper grid.

Diffuse reflectance UV–vis (UV–vis DRS) spectra of the catalysts and the corresponding supports were recorded using a UV-2501 PC Shimadzu spectrometer with an IRS-250A diffusion reflection attachment in the 11000–54000 cm^{-1} range. The measurements were performed in a 2 mm quartz cell in air at room temperature. The UV–vis spectra were transformed into the Kubelka–Munk function ($F(R)$) calculated as $F(R) = (1-R)^2/2R$, where R is the experimentally measured reflectivity coefficient of the samples [31].

Temperature-programmed reduction by H_2 (TPR-H_2) was carried out in a flow reactor. Before the TPR studies, the catalysts were treated in a 20 vol.% O_2/He flow at 450 °C to remove water and carbonates from the surface. The temperature in the reactor was increased from −15 to 450 °C at a rate of 10 °C/min. The flowing gas contained 0.1 vol.% H_2 and 0.5 vol.% Ne with He balance, the flow rate was 100 ml/min, the catalyst granule size was 0.25–0.5 mm and the catalyst loading was 0.2 g.

X-ray photoelectron spectroscopy (XPS) studies were carried out using an ES300 electron spectrometer by Kratos Analytical with MgK_α irradiation ($h\nu$ = 1253.6 eV). For registration of the photoelectron spectra, the samples were ground and deposited on an indium substrate using a flood gun system for neutralization of the sample charging. The spectra were processed using the special software XPS-Spectr, which was previously used for many other systems [32–34]. The spectra were calibrated using the Al2p line of the support, with E_b = 74.5 eV. In this case, the position of the C1s line was 285.0 eV. The chemical composition of the catalysts was calculated using the integral intensities of the lines or their components, subject to the atomic sensitivity factors reported in [35].

Specific surface areas were determined with an accuracy of ±10% through the thermal desorption of argon [36].

Catalytic properties of the synthesized samples were studied in CO oxidation reactions in a temperature-programmed regime (light-off mode). An automatic installation with a flow reactor and mass-spectrometric analysis of the gas phase was used. Catalyst samples with 0.25–0.5 mm grain size were placed in a stainless-steel reactor. The experiments were carried out according to the following procedure. A reaction mixture containing 0.2 vol.% CO, 1.0 vol.% O_2, 0.5 vol.% Ne with He balance was fed to the initial catalyst cooled to −15 °C. The feed flow rate was equal to 1000 cm^3/min. The catalyst was heated in the reaction mixture from −15 to 450 °C at a 10 °C/min heating rate, followed by cooling in the reaction mixture. The concentrations of CO, O_2 and CO_2 were monitored during the reaction. These concentrations were measured at a 0.34 Hz frequency.

3. Results and discussion

3.1. Phase composition and dispersity of the catalysts

Aluminum oxide in the form of γ-Al_2O_3 was used as the support for synthesis of the catalysts containing Pt and Pd. According to the XRD phase analysis data (Fig. 1a), all of the samples consisted of γ-Al_2O_3 with a lattice parameter a = 0.7922 nm and average crystallite size D = 3.5–5.0 nm, which were independent of the calcination temperature. The specific surface area of the Al_2O_3 sample

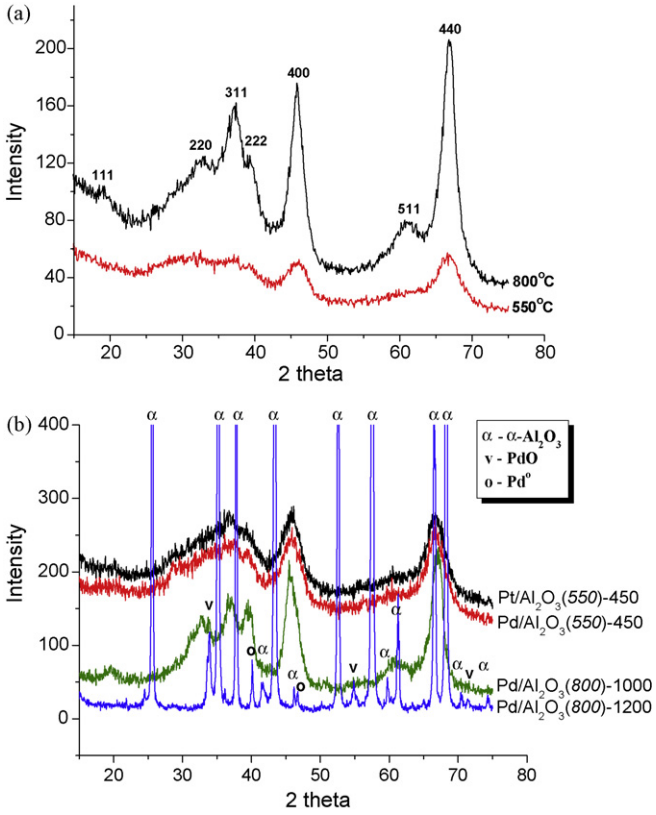

Fig. 1. X-ray diffraction patterns: (a) Al_2O_3(550) and Al_2O_3(800); (b) Pt/Al_2O_3(550)-450, Pd/Al_2O_3(550)-450, Pd/Al_2O_3(800)-1000 and Pd/Al_2O_3(800)-1200 catalysts.

calcined at 550 °C was equal to 300 m^2/g. It was reduced by approximately two times (160 m^2/g) when the calcination temperature was increased from 550 to 800 °C.

The deposition of platinum or palladium on this alumina support did not alter the structure of the support (Fig. 1b). Furthermore, the reflections attributable to the oxide or metal states of the noble metals were not observed in the diffraction profiles. Consequently, it is natural to suppose that the noble metals were in a finely dispersed state after deposition. The phase composition of the catalysts changed only after the calcination at 1000 or 1200 °C (Fig. 1b). A poorly crystallized alumina phase intermediate between γ- and δ-Al_2O_3 and traces of a PdO phase were observed in the XRD profile of the sample Pd/Al_2O_3(800)-1000. Corundum α-Al_2O_3 was the main crystalline phase in the sample Pd/Al_2O_3(800)-1200, with PdO and Pd^o being present as well. The lattice parameter of Pd^o was equal to 0.3891 nm (±0.0003 nm), practically matching the tabulated value (ICDD PDF2 N 00-046-1043). Its particle size was about 70 nm.

3.2. UV–vis study

Diffuse reflectance UV–vis spectra of the 1%Pd/Al_2O_3 catalysts and the Al_2O_3 support are shown in Fig. 2. The spectra of the Al_2O_3(550) and Al_2O_3(800) supports were almost identical. The intensity of the absorption bands in the spectrum of the support (Fig. 2, spectrum a) was substantially lower than in the spectra of the supported catalysts. Thus, two main absorption bands at 20500–25000 cm^{-1} and 33500–49000 cm^{-1} observed in the spectra of the catalysts can be attributed to the d–d transitions and charge-transfers bands (CTB) of Pd^{2+} ions, respectively [37].

The presented spectra show that they substantially depend on the calcination temperatures of both the support and the catalyst. For instance, the spectrum of the catalyst calcined at a low tem-

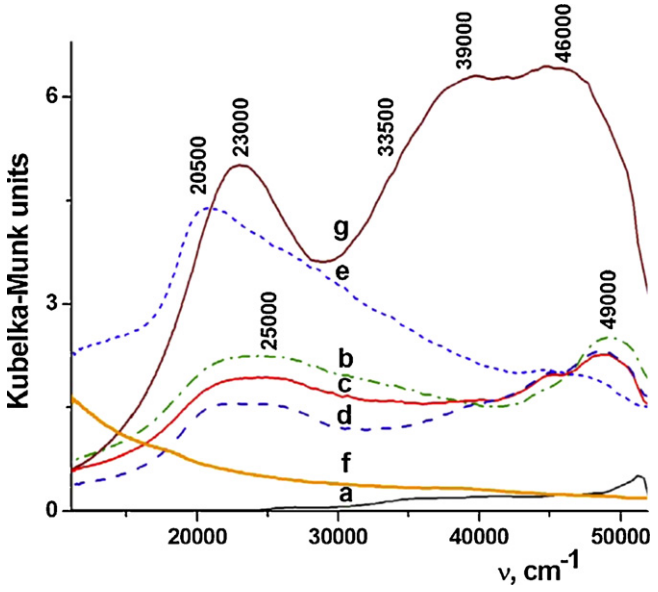

Fig. 2. UV–vis DR spectra of catalysts: Al_2O_3(800) (a); Pd/Al_2O_3(800)-450 (b); Pd/Al_2O_3(800)-600 (c); Pd/Al_2O_3(800)-800 (d); Pd/Al_2O_3(800)-1000 (e); Pd/Al_2O_3(800)-1200 (f); Pd/Al_2O_3(550)-450 (g).

perature, 1%Pd/Al_2O_3(550)-450 (Fig. 2, spectrum g), has the most intense bands at 23000 cm^{-1} and 33000–49000 cm^{-1} and is substantially different from the other spectra.

The presence of absorption bands with such high intensity in both the d–d transition region and the charge-transfer region of the Pd^{2+} ions is unusual for supported palladium catalysts. A similar intensity increase effect was observed for aqueous solutions of palladium chloride complexes [37,38]. It has been shown that the absorption maximum observed at 21100 cm^{-1} corresponds to the spin-allowed d–d transitions of Pd^{2+} ions with the D_{4h} symmetry of $[PdCl_4]^-$ complexes. A shift of the peak position to higher frequencies and the growth of the absorption band intensity were observed after formation of the dimer complexes $[Pd_2Cl_6]^{2-}$ [39]. Consequently, the observation of an intense absorption band at 23000 cm^{-1} in the spectrum of the studied catalysts may correspond to the spin-allowed d–d transitions of Pd^{2+} ions in dimeric square-planar complexes. Also, it should be noted that according to [38], two intense charge-transfer bands at 35600 and 45000 cm^{-1} and a shoulder at 29000 cm^{-1} were observed for square-planar chloride complexes $[PdCl_4]^{2-}$ in aqueous solutions. According to [40], substitution of the chloride environment of the Pd ions for the oxygen environment results in a shift of the charge-transfer band (CTB) to higher frequencies. Apparently, the absorption band at 39000 and 46000 cm^{-1} and shoulder at ~33500 cm^{-1} observed in the spectrum of the Pd/Al_2O_3(550)-450 catalyst can be ascribed to CTB in tetracoordinated Pd^{2+} ions in the oxygen environment.

The high CTB intensity in the spectrum of the studied catalyst may indicate a substantially larger contribution of the palladium ligand environment in comparison with extended bulk or coarsely dispersed PdO. For comparison, let us recall the UV–vis DRS data for PdO. According to [40,41], bulk PdO shows a band in the charge-transfer region at 30200–34500 cm^{-1} (Pd → O) and two other bands in the d–d transition region at 24800 and 20400 cm^{-1}. These data prove that ionic and dimeric palladium exists and strongly interacts with the aluminum oxide.

The catalysts prepared using the support calcined at 800 °C were characterized by a significantly lower intensity of the absorption bands at ~25000 and 49000 cm^{-1} (Fig. 2, spectra b–d). This indicates that the structure and morphology of palladium species on the surface of the support become substantially different when the support calcination temperature was increased. However, the spectra did not show any significant dependence on the catalyst treatment temperature in the range of 450–800 °C, indicating that the catalyst is stable in this temperature range. Nevertheless, some shift of the absorption band attributed to d–d transitions and CTB of Pd^{2+} ions in the D_{4h} oxygen environment in comparison with bulk PdO was observed. In addition, an increase of the calcination temperature to 600–800 °C resulted in changes in the high-frequency spectral region (Fig. 2, spectra c and d). The intensity of the band at 33500 cm^{-1} (metal → ligand CTB) decreased, whereas that of the band at 45000 cm^{-1} (ligand → metal CTB) increased. These changes are apparently related to certain ordering of the oxygen environment of the palladium ions. Finally, the absorption band in the region 21500–25500 cm^{-1} can be attributed to d–d transitions of square-planar polynuclear palladium-oxygen clusters or small PdO clusters [40].

The other characteristic UV–vis spectra appear after high-temperature treatment of the catalysts at 1000 °C. For example, for the sample Pd/Al_2O_3(800)-1000 (Fig. 2, spectrum e), the absorption band in the d–d transition region was shifted to longer wavelengths and the CTB intensity substantially decreased in comparison with that of the d–d transition. The band at 20500 cm^{-1}, according to [41], can be ascribed to bulk PdO particles with no interaction with the support. Thus, catalyst treatment at 1000 °C leads to a substantial decrease of the interaction between the PdO particles and the support, and an increase of their size. Also, it should be noted that the changes of the absorption background in the visible spectral range for this catalyst could be related to strong structureless absorption due to the presence of dispersed palladium metal particles [40] coexisting with PdO.

For the Pd/Al_2O_3(800)-1200 sample (Fig. 2, spectrum f), no absorption bands were observed in the d–d transition and charge-transfer regions of Pd^{2+} ions. Structureless absorption observed in the visible spectral range for this catalyst could be attributed to the presence of large palladium metal particles. Thus, calcination of the Pd/Al_2O_3(800) catalyst at 1200 °C resulted in almost complete reduction of PdO to Pd^0.

Thus, Pd deposition on Al_2O_3 supports calcined at different temperatures leads to the formation of different types of the palladium surface compounds and particles on the surface of the γ-Al_2O_3 support, including both individual palladium metal and oxide forms, as well as mixed surface aluminate compounds and phases. For example, palladium–aluminate is formed on the surface of the Pd/Al_2O_3(550)-450 sample. Finely dispersed PdO predominates on the surfaces of Pd/Al_2O_3(800)-450, Pd/Al_2O_3(800)-600 and Pd/Al_2O_3(800)-800. An increase of the catalyst calcination temperature to 1000–1200 °C resulted in the growth of PdO particles and gradual transformation of PdO → Pd^0.

3.3. HRTEM study of the catalysts

According to the HRTEM data (Fig. 3), the samples of supported catalysts with different support and catalyst calcination temperatures were characterized by substantial changes of the support morphology. Fig, 3 shows the results of the support morphology investigation for the palladium–alumina system Pd/Al_2O_3. The particles of the 1%Pd/Al_2O_3(550)-450 catalyst were porous crystalline aggregates with dimensions of 100 nm or more, consisting of needle-shaped blocks with d = 5–10 nm and l = 20–50 nm (Fig. 3a). An increase of the catalyst calcination temperature to 800–1000 °C resulted in support sintering, as reflected in the significant changes in its morphology (Fig. 3b and c). When the calcination temperature was increased to 1200 °C, the support experienced substantial changes due to its transformation to the α-Al_2O_3 phase. This resulted in the appearance of large α-Al_2O_3 particles with dimensions from 100 to 500 nm in the HRTEM-images (Fig. 3d).

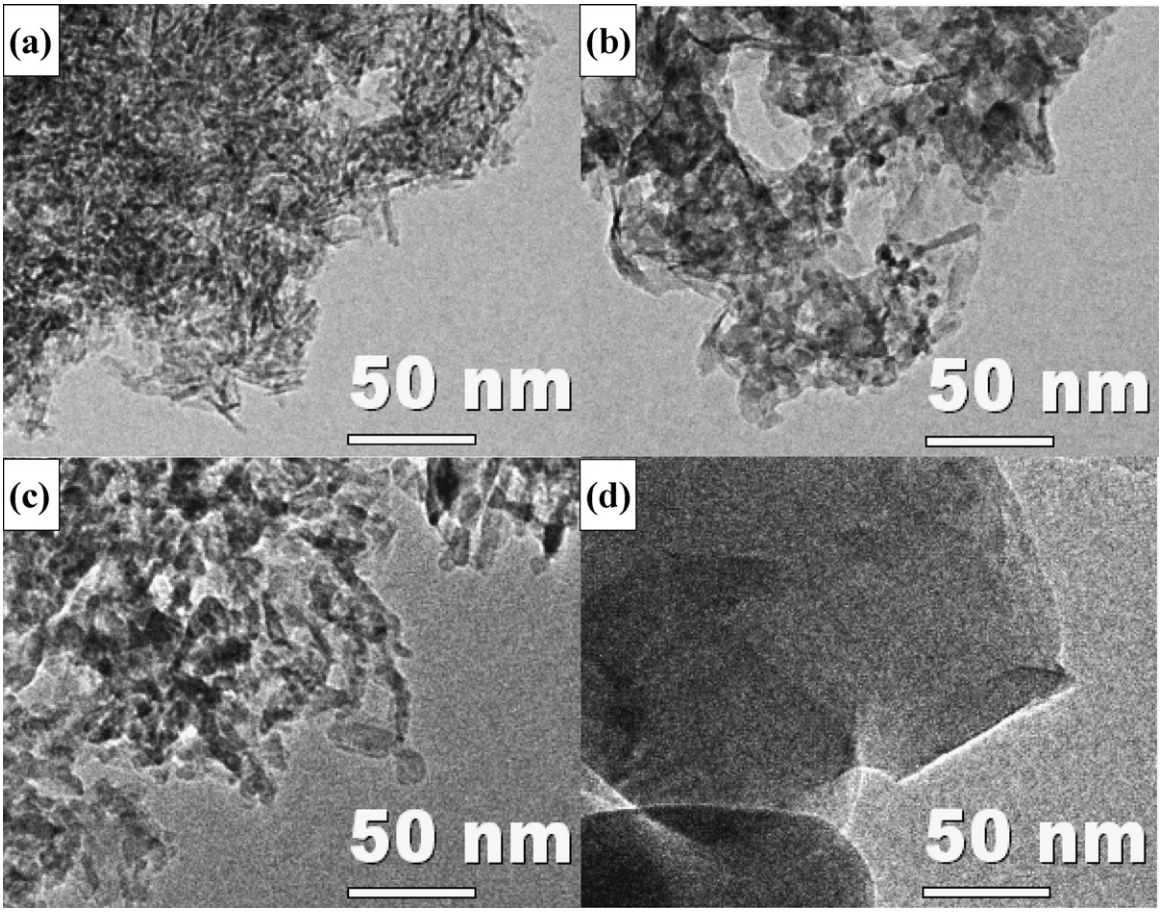

Fig. 3. Morphology of the Al_2O_3 particles in the catalysts Pd/Al_2O_3(550)-450 (a); Pd/Al_2O_3(550)-800 (b); Pd/Al_2O_3(800)-1000 (c) and Pd/Al_2O_3(800)-1200 (d).

The particles of the supported metal in the Pt/Al_2O_3(550)-450 and Pd/Al_2O_3(550)-450 catalysts were dispersed on the support surface. One can see (Fig. 4) that platinum is irregularly distributed on the Al_2O_3 surface. The particles of the supported component were observed in some regions of the support, while being totally absent in others. The EDX spectrum (Fig. 4b) obtained from region 1 (Fig. 4a) showed that no platinum was present in this part of the surface. Some platinum existed as large particles (PtO_x, probably in an amorphous state) with dimensions of about 100 nm (Fig. 4a, region 2). This was also supported by the EDX spectrum (Fig. 4b, region 2). The remaining platinum was observed in the HRTEM-image (Fig. 4c, region 3) in the form of agglomerated metal clusters with dimensions of 1.5–2 nm. Fig. 4d shows the HRTEM-image of the Pt cluster after the Fourier processing, and the Fourier image obtained for this cluster with identification of the reflections from Pt^0. An increase of the Pt/Al_2O_3 catalyst treatment temperature to 600 °C resulted in better crystallization of the platinum particles. Large PtO_x particles were transformed into metal particles (Fig. 5, Table 1), as shown in the microdiffraction image (Fig. 5c). Fig. 5a and b shows that both large particles with dimensions about 40 nm (Fig. 5b, region 1) and Pt metal clusters (Fig. 5b, region 2) were present in this catalyst.

Palladium particles in the Pd/Al_2O_3(550)-450 catalyst (Fig. 6) were also distributed irregularly, as in the Pt/Al_2O_3(550)-450 catalyst discussed above. Both individual and aggregated particles were present. The individual Pd particles were about 2–3 nm in size. In contrast to the platinum particles, the surface of the palladium particles was almost completely covered by a thin Al_2O_3 layer, i.e., they were decorated by the support. The dimensions of the aggregated particles did not exceed 100 nm. Table 1 shows that the dimensions of the particles in the catalysts Pt/Al_2O_3(550)-450 and Pd/Al_2O_3(550)-450 were 1–2 and 2–3 nm for Pt and Pd, respec-

Table 1
Catalyst characteristics according to HRTEM data.

Sample	Surface concentration, atom Pt(Pd)/nm^2	Calcination temperature, °C		Particles size, nm	
		Support	Catalyst	Crystallites	Aggregates
Pt/Al_2O_3	0.106	550	450	1–2	~100
	0.106	550	600	1–2	~40
Pd/Al_2O_3	0.197	550	450	2–3	~100
Pd/Al_2O_3	0.371	800	450	2–3	≤20
		800	600	3–4	≤50
		800	800	3–7	<100
		800	1000	2–3	20–100
		800	1200	≥200	–

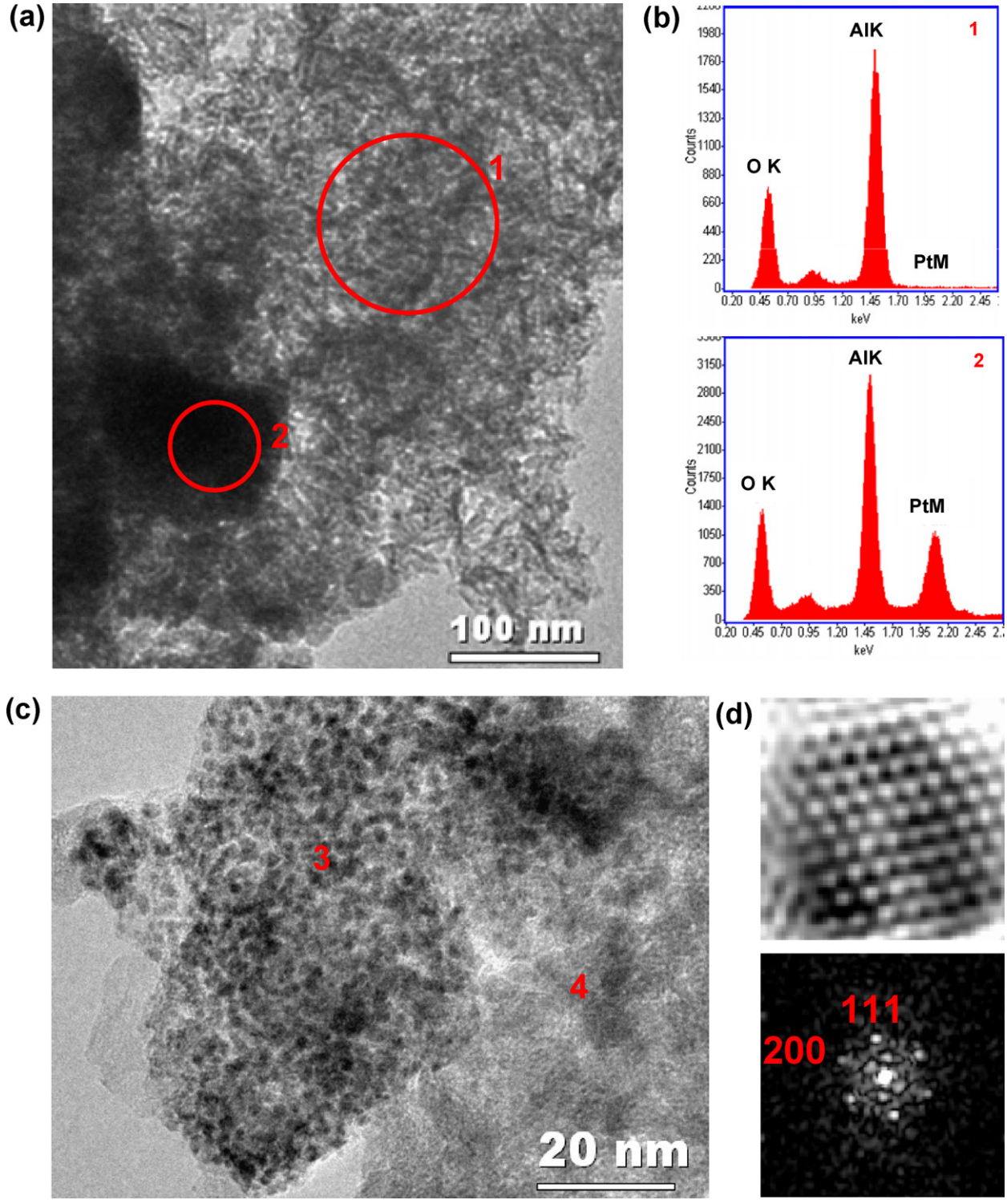

Fig. 4. TEM images of Pt/Al_2O_3(550)-450 catalyst: (a) «pure» support (region 1), PtO_x particles (region 2); (b) EDX-spectra from regions 1 and 2, respectively; (c) agglomeration of the Pt metallic clusters (region 3), support without Pt (region 4); (d) HRTEM-image of the single Pt cluster and FFT from the cluster with the indication of patterns.

tively. The observed differences in the dimensions of the Pt and Pd particles are probably due to their different surface concentrations (Table 1).

An increase of the support calcination temperature to 800 °C did not have a significant influence on the particle distribution, but resulted in changes of their dimensions in the Pd/Al_2O_3(800)-450 catalyst (Fig. 6c and d). The individual and aggregated particles were also present on the surface, with sizes varying between 2–3 and 10–20 nm, respectively. Thus, the aggregated particles formed on the surface of the support calcined at higher temperature were about 5–10 times smaller than in the sample calcined at 550 °C. Additionally, the surface concentration of palladium grew by roughly a factor of 3 (Table 1). The aggregated Pd particles consisted of crystallites with dimensions of about 2–4 nm connected at the dislocation boundaries. It should be noted that the predominant part of the metal surface was covered by an Al_2O_3 layer in this

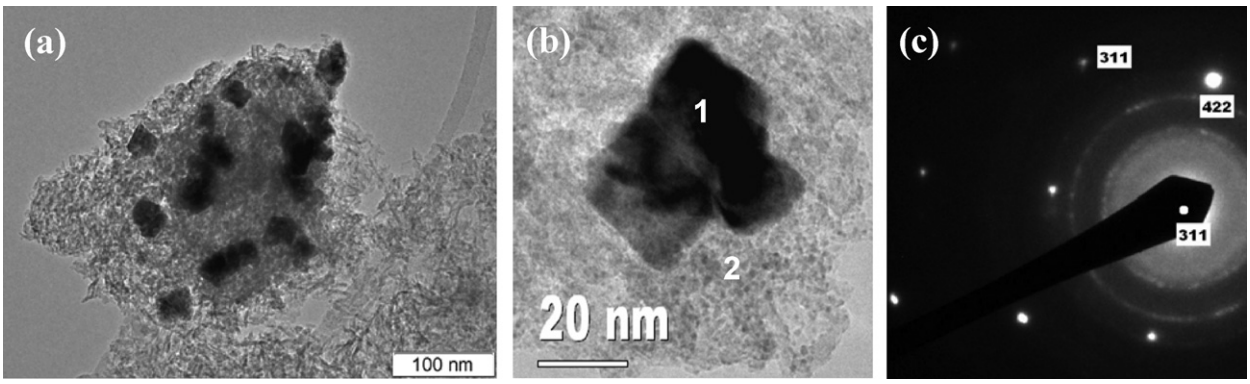

Fig. 5. Pt^0 particles in the Pt/Al_2O_3(550)-600 catalyst (a); HRTEM-image (b): region 1—Pt^0 particles ~40 nm, region 2—aggregation of Pt^0 clusters; SAED from the particles (b, region 1) with indication of the patterns from Pt^0 (c).

catalyst. So, palladium is oxidized from the side of contact with the Al_2O_3 surface with a shift from the initial surface. In addition, small palladium particles were epitaxially bound with the surface of the (1 1 1) Al_2O_3 face (Fig. 6e and f). Taking into account the results obtained by UV–vis DRS, we cannot exclude the formation of palladium–aluminate at the palladium–alumina interface boundary (Fig. 6c and d). The palladium interaction with the γ-Al_2O_3-800 surface resulted in encapsulation of the palladium particles by the support. In the formed core-shell structures, the core was made of palladium metal, and the shell consisted of palladium–aluminate. A small increase of the particle size of the palladium nanoparticles and agglomerates was observed for the catalysts calcined at higher temperatures, such as Pd/Al_2O_3(800)-600 and Pd/Al_2O_3(800)-800 (Table 1). Additionally, the epitaxy of the palladium particles with the alumina surface was also preserved. In other words, the morphology of the palladium particles and interaction with the surface in general were preserved and were in agreement with the data obtained by UV–vis DRS. Thus, the HRTEM-images of these catalysts were not reported.

For further analysis of the effects of the catalyst treatment, the HRTEM-images of the Pd/Al_2O_3(800)-1000 catalyst before reaction and after CO oxidation in the unsteady-state light-off mode with cyclic catalyst heating in the reaction mixture up to 450 °C are presented in Fig. 7. One can see finely dispersed Pd^0 metal particles with dimensions of 2–3 nm (Fig. 7a) and aggregates of PdO particles with dimensions of 20–100 nm (Fig. 7b) on the alumina surface in the initial sample. After the CO oxidation, the large PdO particles were preserved. Meanwhile, the fraction of small Pd clusters substantially increased (Fig. 7c). It should be noted that the palladium dispersion was accompanied by decoration of small Pd^0 particles with aluminum oxide (Fig. 7d).

Fig. 8 presents HRTEM-images of the Pd/Al_2O_3(800)-1200 catalyst before (Fig. 8a) and after the reaction (Fig. 8b). One can see that large palladium metal particles with dimensions of about 200 nm predominated in the initial catalyst. According to the XRD data, their average crystallite size was about 70 nm. The difference between the results of the two methods is probably related to agglomeration of the primary metal particles into aggregates. It is interesting that after the CO oxidation reaction, the large metal particles on the alumina surface experienced significant changes. These particles were cracked to form smaller Pd^0 and PdO particles on the support surface (Fig. 8b).

3.4. Temperature-programmed reduction in hydrogen (TPR-H_2)

Fresh Pt/Al_2O_3(550)-450 and Pd/Al_2O_3(550)-450 samples containing 52.8 μmol Pd/g and 95.9 μmol Pt/g, respectively, were studied by TPR-H_2 at low H_2 concentration (0.1 vol.%) and a high flow rate. These conditions were chosen because the sensitivity is inversely proportional to the hydrogen concentration [42]. According to the obtained results (Fig. 9a), two stages were identified during the platinum oxide reduction. Two reduction peaks at 44 and 85 °C were observed in the reduction profile of the Pt/Al_2O_3 sample. The presence of the two peaks in the TPR-H_2 spectrum of this sample could be related to different dispersions of platinum oxide, which is in agreement with the HRTEM results. The ratio of the consumed hydrogen to Pt was about 2.2. Hence, platinum on the surface of the support is in the oxidized state close to PtO_2.

A completely different type of reduction was observed for the Pd/Al_2O_3(550)-450 sample (Fig. 9a). No distinct maximum was observed in the TPR-H_2 profile of this sample, and reduction took place over the whole temperature range from 0 to 450 °C without showing any structural features. This means that no oxidized palladium structures were reduced in this temperature range. Taking into account the data obtained by UV–vis DRS (Fig. 2), the observed structureless reaction with hydrogen could be related to the interaction of hydrogen with non-stoichiometric palladium–aluminate compounds decorating the palladium metal islands (Fig. 6). The increase of the support calcination temperature to 800 °C altered the character of reduction for the Pd/Al_2O_3(800)-450 sample (Fig. 9b). Two peaks with maxima at 48 and 64 °C were observed in the TPR-H_2 profile. Similar results were obtained in [43], where a single reduction peak at 55 °C was observed for the Pd/γ-Al_2O_3 sample. The appearance of the second peak in the profile in our experiments could be due to the low hydrogen concentration (0.1 vol.%) and higher flow rate (100 cm^3/min) (compared to 10 vol.% H_2 and 15 cm^3/min flow rate in [43]), which increases the method sensitivity [42]. In [44], the two peaks observed during the PdO reduction were attributed to the presence of two oxide phases having different interactions with the support. Smaller PdO particles interacted more strongly with the support, thus resulting in a higher reduction temperature. A similar conclusion was also made in [45], where a more complex reduction profile was attributed to different types of the Pd–support interactions.

The molar ratio of consumed H_2 to Pd for the studied catalyst was 1.09. Therefore, the main state of palladium on the surface of the support was PdO. Apparently, the second reduction peak was related to reduction of the oxide clusters, whereas the first one corresponded to reduction of PdO aggregates.

Two peaks were also observed in the TPR-H_2 profile of the Pd/Al_2O_3(800)-800 sample calcined at higher temperatures (Fig. 9b). In this case, the maxima of the peaks were at 23 and 42 °C, whereas the ratio of consumed H_2 to Pd in the catalyst was 0.55. These data indicate that an increase of the calcination temperature to 800 °C leads to palladium stabilization in two states, Pd^0 and PdO, in approximately equal concentrations.

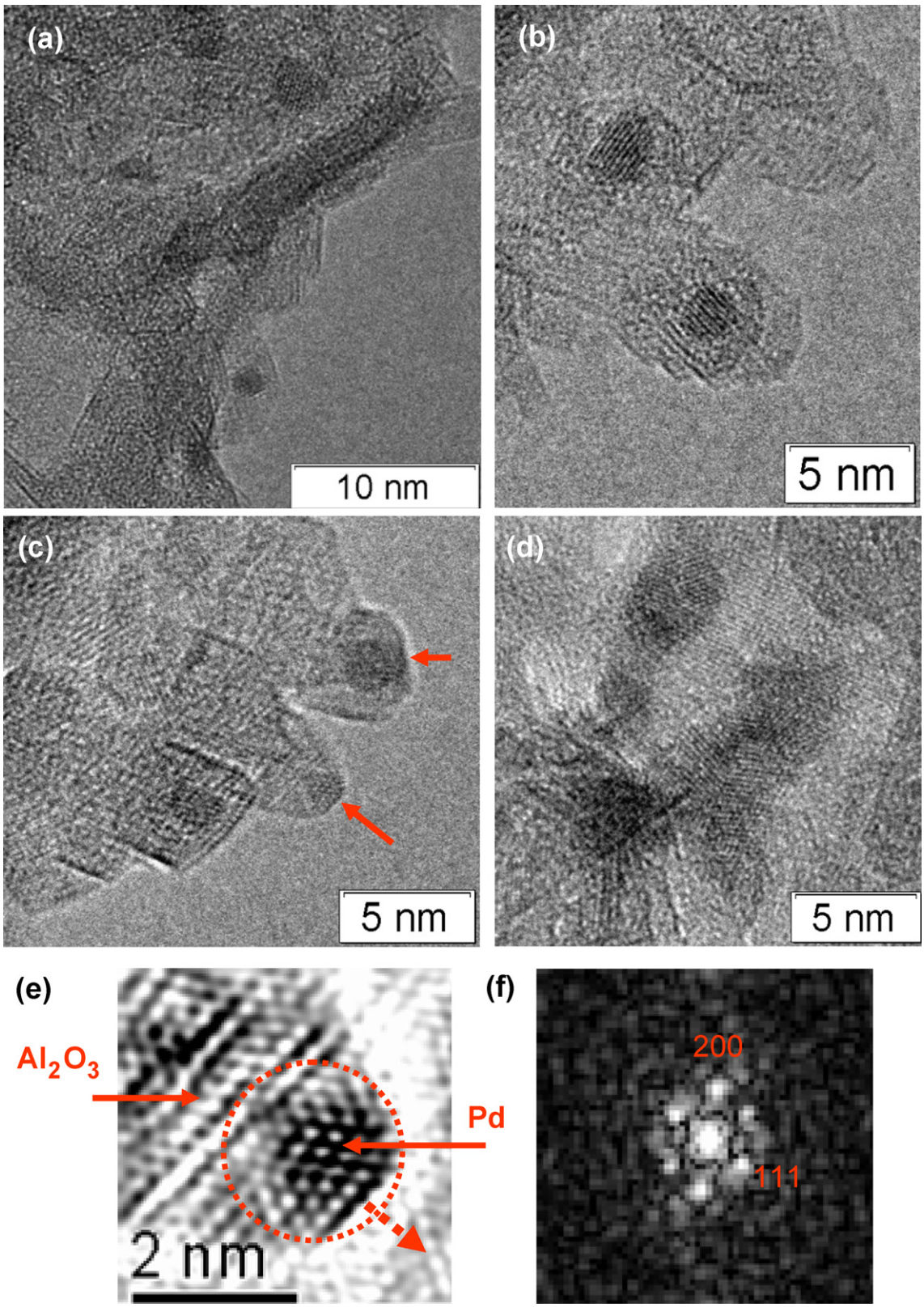

Fig. 6. HRTEM-images of the catalysts: Pd/Al_2O_3(550)-450, individual Pd particles with sizes of about 2–3 nm (a); the surface of metallic Pd particles were totally covered by a thin layer of Al_2O_3 (b); Pd/Al_2O_3(800)-450; (c) individual Pd particles (arrows show area of the metallic surface without a layer of Al_2O_3); (d) aggregate of the Pd crystallites; (e) HRTEM-image of the single Pd cluster with epitaxial bonding of Pd particles on Al_2O_3 (dashed arrow shows coincident direction [1 1 1] for Pd and Al_2O_3; (f) FFT from cluster with indication of Pd^o patterns.

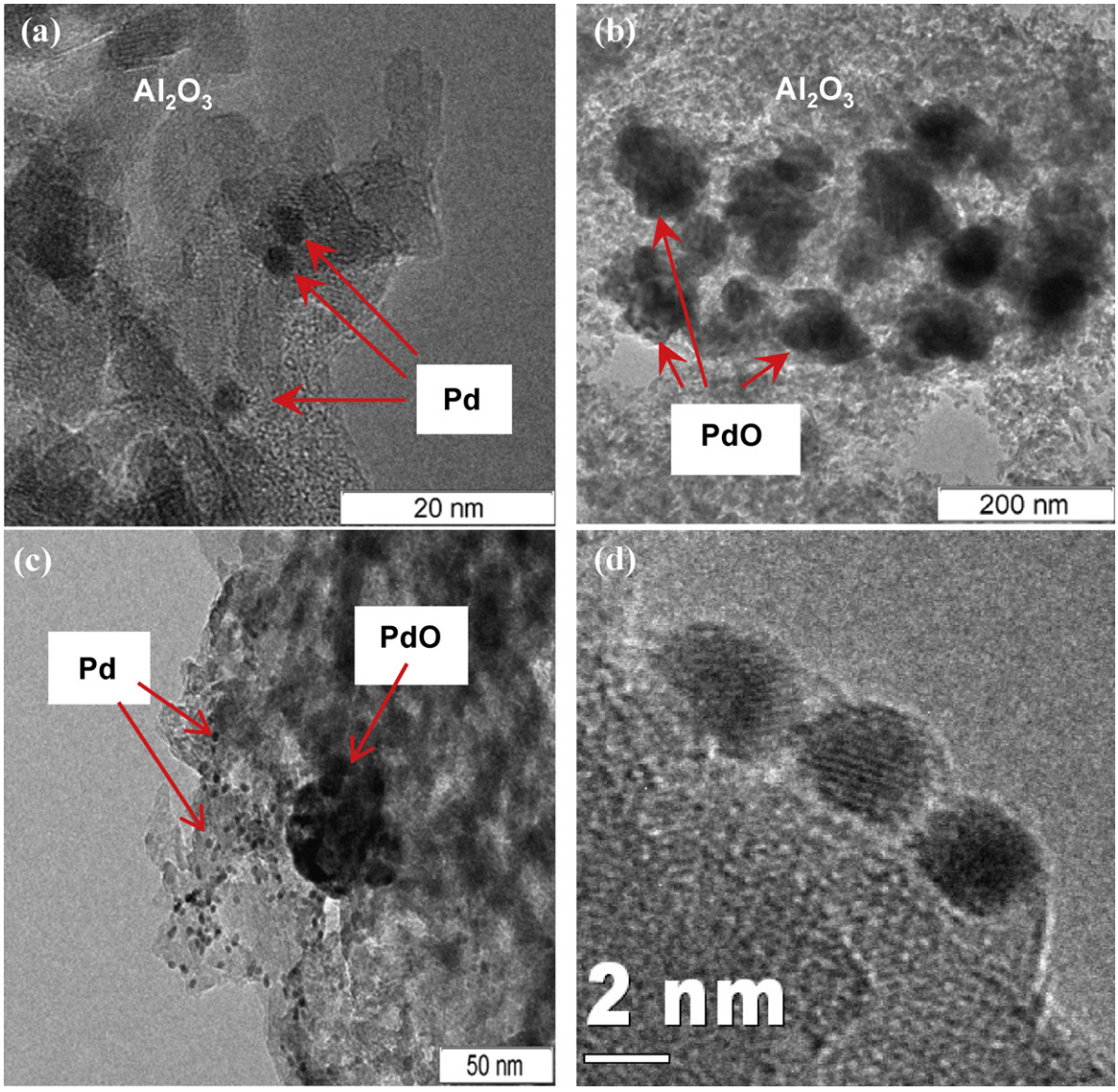

Fig. 7. TEM images of $Pd/Al_2O_3(800)$-1000 catalyst: (a and b) fresh catalyst; (c and d) catalyst after action of the reaction mixture; (a) highly dispersed particles of Pd^o (2–3 nm); (b) aggregates of PdO particles (20–100 nm); (c) large particles of PdO (50–100 nm) and agglomerates of Pd^o particles (2–3 nm); (d) small Pd^o particles decorated by alumina.

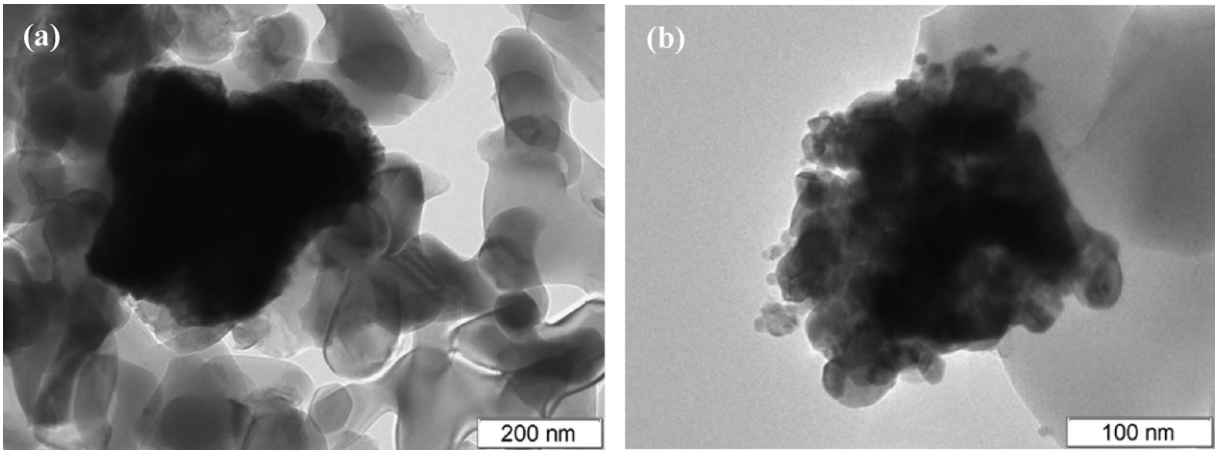

Fig. 8. TEM image of $Pd/Al_2O_3(800)$-1200 catalyst: (a) fresh catalyst; (b) after action of the reaction mixture. The large Pd^o particles (~200 nm) were observed both in the fresh catalyst and in the catalyst after reaction. The surface of the Pd particles was cracked after treatment with the reaction mixture.

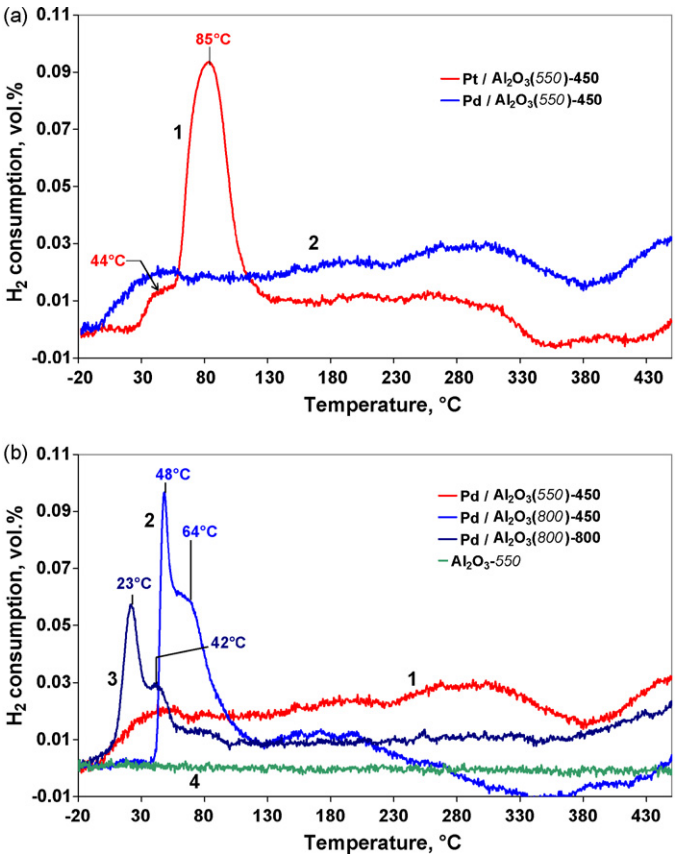

Fig. 9. The dependence of H_2 consumption during TPR-H_2 for catalysts: (a) Pt/Al_2O_3(550)-450 (1) and Pd/Al_2O_3(550)-450 (2); (b) Pd/Al_2O_3(550)-450 (1), Pd/Al_2O_3(800)-450 (2), Pd/Al_2O_3(800)-800 (3), Al_2O_3(550) (4).

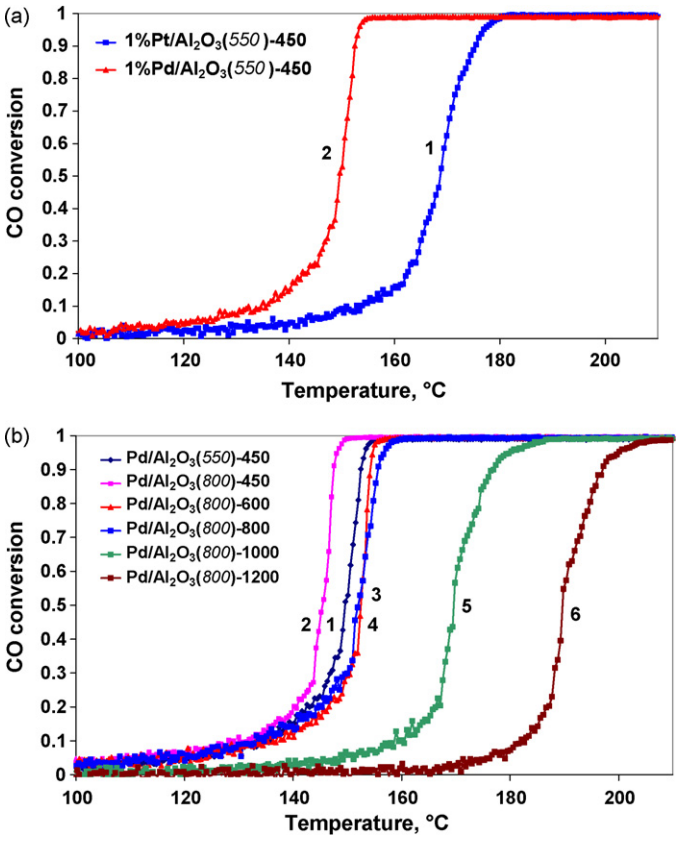

Fig. 10. Temperature dependence of the CO conversion for catalysts: (a) Pt/Al_2O_3 (1) and Pd/Al_2O_3 (2); (b) Pd/Al_2O_3(550)-450 (1), Pd/Al_2O_3(800)-450 (2), Pd/Al_2O_3(800)-600 (3), Pd/Al_2O_3(800)-800 (4), Pd/Al_2O_3(800)-1000 (5), Pd/Al_2O_3(800)-1200 (6).

Therefore, a decrease of the reduction temperature with an increase of the catalyst calcination temperature from 450 to 800 °C is apparently due to weakening of the Pd interaction with the support. In this case, the increase of the calcination temperatures for both the support and the catalyst results in transformation of the strongly bound encapsulated (decorated with the support) palladium to the oxidized state (PdO), and then to a mixture of the oxidized and partially reduced states PdO and Pd^0.

3.5. Investigation of the catalytic properties in CO oxidation by the light-off method

The catalytic properties of Pd/Al_2O_3 and Pt/Al_2O_3 for CO oxidation were determined by the temperature-programmed (light-off) method. The conversion followed a typical light-off process for CO oxidation over Pd(Pt), which can be divided into three different temperature regions. At low temperatures, the reaction is self-inhibited by a high coverage of the active sites with CO [46,47], and the conversion is therefore very low. At higher temperatures, the CO conversion is high and the surface coverage with CO is low. In this region, the reaction rate is limited by the transport of reactants to the catalyst active sites. In the intermediate light-off region, the reaction rate can be enhanced during the heating ramp by the evolved reaction heat, which results in a rapid increase from low to high conversion.

The Pt/Al_2O_3(550)-450 catalyst is the slightly lower active than the Pd/Al_2O_3(550)-450 catalyst (Fig. 10a, Table 2). The reaction started at 100 °C on both catalysts. The temperatures corresponding to 10% CO conversion (T_{10}) were 145 and 154 °C for Pd/Al_2O_3 and Pt/Al_2O_3, respectively. The respective T_{50} temperatures were 155 and 169 °C, and the T_{90} temperatures were 163 and 176 °C. Thus, the range of temperatures where the CO conversion increases from 10% to 90% on the studied catalysts was 18–22 °C.

The increase of the catalyst or support calcination temperature to 800 °C had practically no effect on the character of CO oxidation (Fig. 10b, Table 2). An increase of the support calcination temperature to 800 °C resulted in a decrease of T_{50} to 145 °C. An increase of the catalyst calcination temperature from 450 to 800 °C resulted in a slightly decrease of T_{50} to 152 °C. The most significant changes leading to a sharp decrease of CO conversion took place after a further increase of the calcination temperature. For the catalysts calcined at 1000 and 1200 °C, T_{50} was 169 and 189 °C, respectively. Thus, Pd/Al_2O_3(800)-450 was the most active among the studied palladium catalysts. Overall, only the catalysts with the support and catalyst calcination temperatures not exceeding 800 °C were active.

As a concluding remark to this part of our study, let us note that the Al_2O_3 support itself did not show CO conversion up to ~350 °C.

Table 2
Catalytic properties.

Catalyst	T_{10}, °C	T_{50}, °C
Pt/Al_2O_3(550)-450	154	169
Pd/Al_2O_3(550)-450	135	150
Pd/Al_2O_3(800)-450	130	145
Pd/Al_2O_3(800)-600	135	152
Pd/Al_2O_3(800)-800	135	152
Pd/Al_2O_3(800)-1000	160	169
Pd/Al_2O_3(800)-1200	182	189

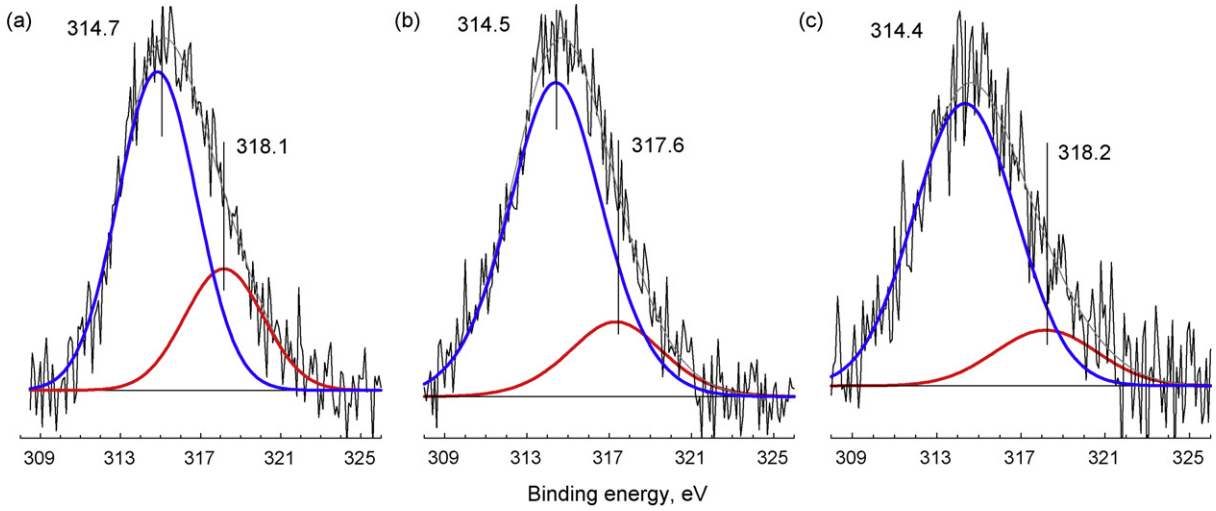

Fig. 11. Decomposition of the $Pt4d_{5/2}$ line on individual Gauss-Lorentz components. Pt/Al_2O_3 catalyst: (a) initial (before $CO + O_2$ reaction treatment); (b) after $CO + O_2$ reaction treatment; (c) after reduction by H_2.

3.6. XPS study of the catalysts

3.6.1. XPS study of calcined catalysts

XPS was used to determine the chemical state of the active components in the synthesized catalysts. First, let us note a known problem in the XPS study of Pt/Al_2O_3 catalysts. The Al2p line of the support overlaps with the Pt4f line of the active component usually used for the spectroscopic analysis of platinum. This makes direct analysis of the platinum states very complicated. Therefore, in this study we used a different line, Pt4d. Although this line is weaker, it is not overlapped by the spectral lines of the other components.

Fig. 11 presents the spectral region of the $Pt4d_{5/2}$ line with subtraction of the background spectrum from scattered electrons approximated using Shirley's method [48]. The decomposition of the spectra to individual components revealed the presence of two platinum states in the catalysts: the reduced (metal) state with $E_b(Pt4d_{5/2}) = 314.4–314.7$ eV and the oxidized state with $E_b(Pt4d_{5/2}) = 317.6–318.2$ eV [49–52]. The intensity of the signal corresponding to the oxidized state decreased after treatment with the reaction mixture of $CO + O_2$ (Fig. 11a and b), indicating the reduction of platinum oxide. Meanwhile, treatment in hydrogen resulted in almost complete reduction of the oxidized platinum to

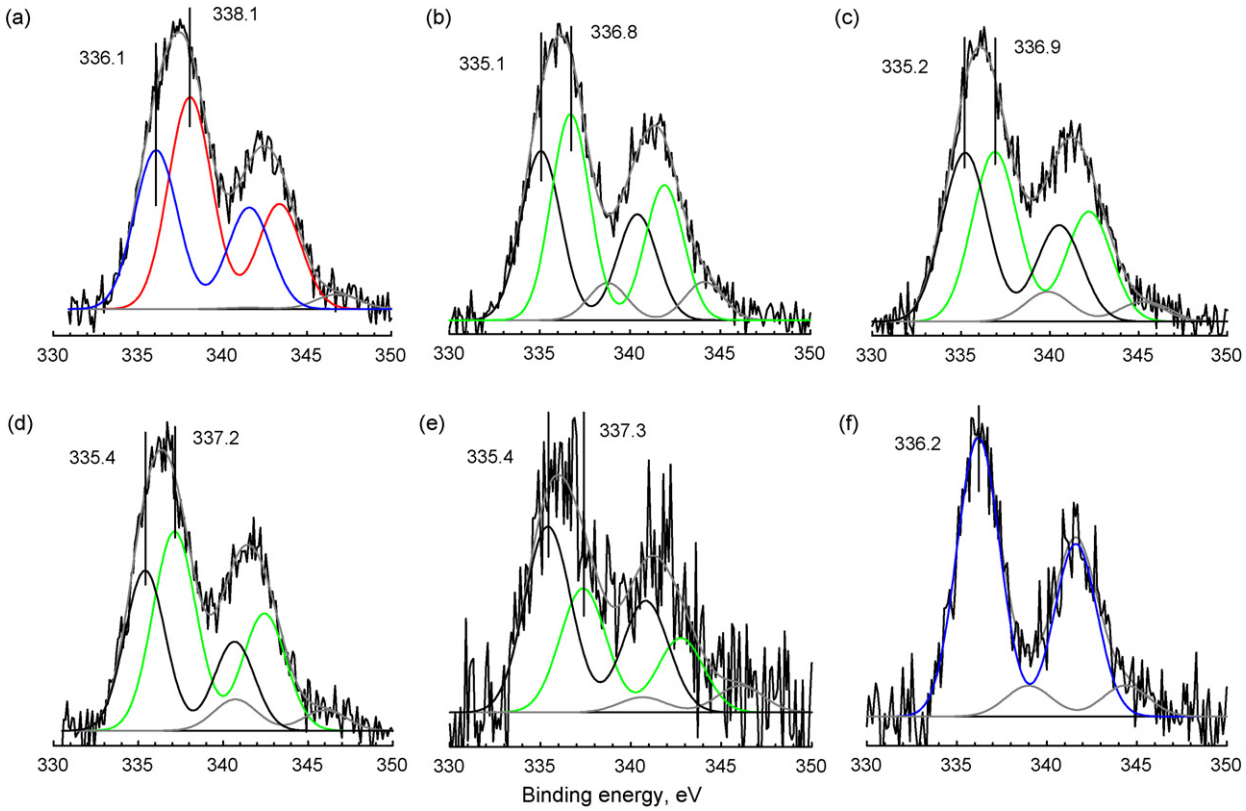

Fig. 12. Pd3d spectra obtained for initial calcined catalysts. (a) $Pd/Al_2O_3(550)$-450; (b) $Pd/Al_2O_3(800)$-450; (c) $Pd/Al_2O_3(800)$-600; (d) $Pd/Al_2O_3(800)$-800; (e) $Pd/Al_2O_3(800)$-1000; (f) $Pd/Al_2O_3(800)$-1200.

platinum metal (Fig. 11c). It should be noted that the fraction of the oxidized state in the spectrum may not correspond to the real concentration of platinum oxide, because according to the HRTEM data, platinum oxide existed in the form of large particles. The signal intensity in XPS is known to be determined by the dispersity of the sample, in addition to other factors. It is higher when the sample has a finer dispersity. Thus, small metal clusters can have a more intense signal than large oxide particles, even if the concentration of the former is lower.

The XPS spectra of the catalysts Pd/Al_2O_3(550)-450, Pd/Al_2O_3(800)-450, Pd/Al_2O_3(800)-600, Pd/Al_2O_3(800)-800, Pd/Al_2O_3(800)-1000 and Pd/Al_2O_3(800)-1200 are shown in Fig. 12. The deconvolution of the spectra to individual components showed that there were two forms of palladium on the surface of all samples corresponding to the oxidized state with $E_b(Pd3d_{5/2}) \sim 337–338$ eV and the reduced state with $E_b(Pd3d_{5/2}) \sim 335–336$ eV. The doublets with larger E_b correspond to the plasmon losses and are not discussed here.

According to the literature data [35,53–58], palladium supported on Al_2O_3 may exist in three forms (Pd^0, PdO and PdO_2) or a combination thereof. The binding energies of the Pd3d line in these compounds are in narrow ranges equal to $E_b(Pd3d_{5/2}) = 335.1–335.4$ eV for Pd^0 [35,53,54], $E_b(Pd3d_{5/2}) = 336.8–337.2$ eV [35,53,55] or 336.3–336.8 eV [56,57] for PdO and $E_b(Pd3d_{5/2}) = 337.8–339.3$ eV for PdO_2 [59–62].

The $E_b(Pd3d_{5/2})$ values observed for the Pd/Al_2O_3(550)-450 sample (Fig. 12a) were equal to 336.1 and 338.1 eV, and did not correspond to the standard values for the metal and oxidized states of palladium. The value $E_b(Pd3d_{5/2}) = 336.1$ eV observed for reduced palladium was in between Pd^0 and PdO. In agreement with the UV–vis DRS and TPR-H_2 results, this component apparently corresponds to small palladium clusters. Its shift to larger E_b values is due to the small sizes of the particles [63–65]. This is in agreement with the HRTEM data showing the presence of metal clusters with dimensions of 1.5–2 nm on the surface of this catalyst. These clusters are epitaxially bound to the support surface and covered with an aluminum oxide layer consisting of the palladium–aluminate compound at the palladium–alumina interface boundary. The position of the second doublet in the Pd3d spectrum with $E_b(Pd3d_{5/2}) = 338.1$ eV is in perfect agreement with the formation of palladium–aluminate structures.

The XPS spectra of Pd/Al_2O_3(800)-450 (Fig. 12b) showed signals with $E_b(Pd3d_{5/2}) = 335.1$ and 336.8 eV, corresponding to palladium in the reduced (Pd^0) and oxidized (PdO) states, with a prevalence of the second one. An increase of the calcination temperature of the Pd/Al_2O_3(800)-450 catalyst to 600 °C (Pd/Al_2O_3(800)-600), 800 °C (Pd/Al_2O_3(800)-800) and 1000 °C (Pd/Al_2O_3(800)-1000) (Fig. 12c–e) was accompanied by a steady growth of the $E_b(Pd3d_{5/2})$ values from 335.1 to 335.4 eV for Pd^0 and from 336.8 to 337.3 eV for PdO. Most likely, this shift is caused by the growth and ordering of the metal and oxide palladium particles, which is in agreement with the TEM and TPR-H_2 data. Interesting data were obtained for the catalyst calcined at 1200 °C. Only one state of palladium with $E_b(Pd3d_{5/2}) = 336.2$ eV was observed for this catalyst (Fig. 12f). This value is in between the metal and PdO oxide states. However, there is no doubt that this state corresponds to palladium metal. At temperatures exceeding 1000 °C palladium oxide is reduced to metal, as is clearly shown by the HRTEM and UV–vis DRS data. Still, the position of the Pd3d line did not match the usual one for the metal state. Most likely, this shift is related to the differential charging effects in XPS spectroscopy rather than to the initial oxidation state of palladium. As this sample consists of a mixture of large sintered palladium particles and large α-Al_2O_3 particles, the contact between the particles is weak due to their large size. Therefore, different

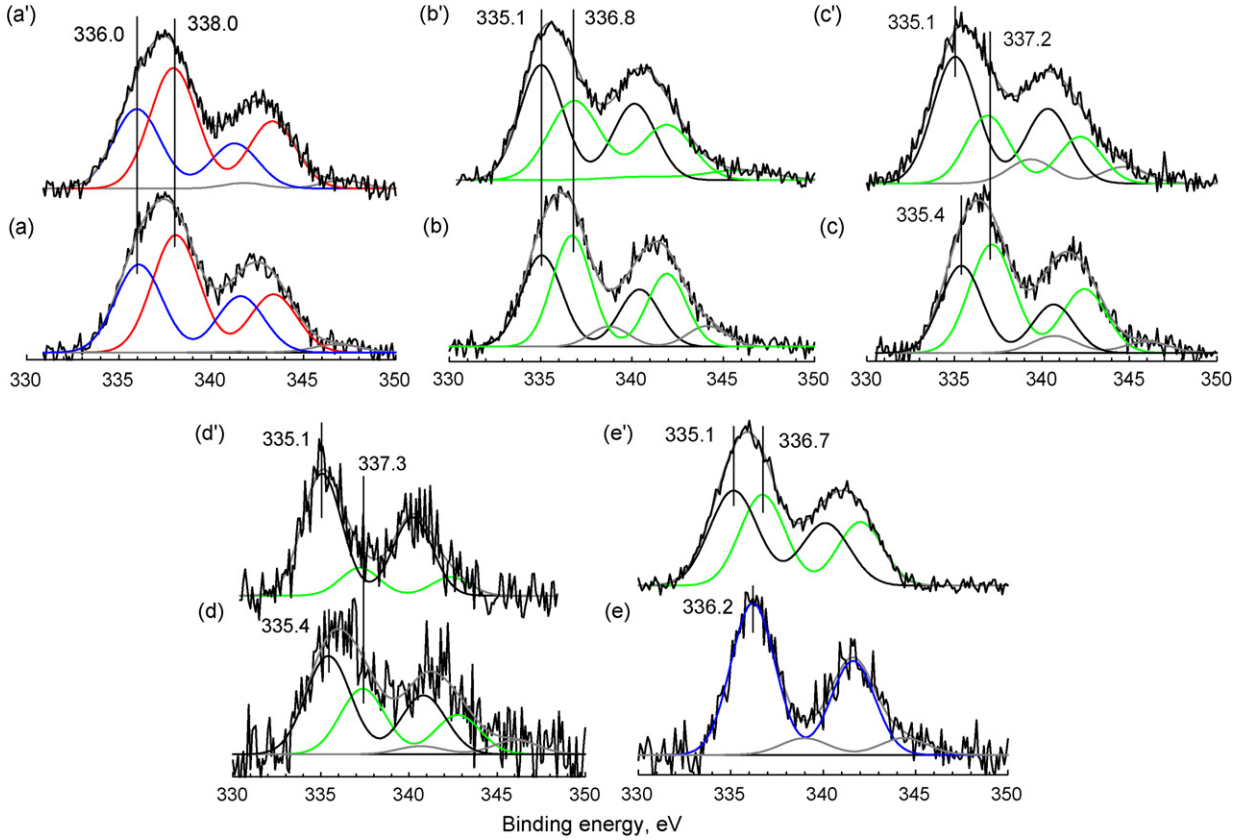

Fig. 13. Pd3d spectra obtained for the catalysts: (a and a′) Pd/Al_2O_3(550)-450; (b and b′) Pd/Al_2O_3(800)-450; (c and c′) Pd/Al_2O_3(800)-800; (d and d′) Pd/Al_2O_3(800)-1000; (e and e′) Pd/Al_2O_3(800)-1200; a–e—calcined catalysts (before $CO + O_2$ reaction treatment); a′–e′—after $CO + O_2$ reaction treatment).

electrostatic potentials determined by the ability of the substances to capture secondary electrons are induced on the surfaces of the palladium and aluminum oxide. This potential is larger on the surface of the palladium particles than on that of the support. So, the position of the Pd3d line is shifted to 336.2 eV.

3.6.2. Investigation of the catalysts treated with the reaction mixture

Investigation of the catalysts treated with the reaction mixture was carried out for the palladium catalysts. The reaction was carried out by cyclic heating of the sample in a $CO + O_2$ mixture ($p(CO)/p(O_2) = 1/5$) to 450 °C and back to room temperature. The light-off curves obtained during this cyclic heating are reported above in Fig. 10. Fig. 13 presents the Pd3d spectra obtained before and after the reaction for the key catalysts Pd/Al_2O_3(550)-450, Pd/Al_2O_3(800)-450, Pd/Al_2O_3(800)-800, Pd/Al_2O_3(800)-1000 and Pd/Al_2O_3(800)-1200. The results reported in Fig. 13 show that treatment in the reaction mixture had different effects on the studied catalysts.

First, note that the only catalyst where the state of palladium was not affected by treatment with the reaction mixture was Pd/Al_2O_3(550)-450 (Fig. 13a and a′). This observation proves the hypothesis of the strong interaction of the palladium particles with the surface of the support in this sample stabilizing the morphology and composition of the particles. As was discussed above during presentation of the HRTEM data, this stabilization is due to the formation of the epitaxial Pd^0–support bond and the decoration effect.

The catalysts prepared using the support calcined at 800 °C showed similar behavior after the reaction (Fig. 13 b, b′, c, c′, d and d′). After the samples Pd/Al_2O_3(800)-450, Pd/Al_2O_3(800)-800, Pd/Al_2O_3(800)-1000 containing both the metal and oxide particles on the surface were treated with the reaction mixture $CO + O_2$, the fraction of palladium in the metal state grew, whereas the concentration of the PdO oxide decreased. Simultaneous existence of palladium in the forms of metal and oxide nanoparticles is typical of the catalysts Pd/Al_2O_3(800)-450 and Pd/Al_2O_3(800)-800 having high catalytic efficiency (Fig. 10b). The intensity of the PdO components in the catalyst Pd/Al_2O_3(800)-1000 after the reaction was substantially lower than in the catalysts Pd/Al_2O_3(800)-450 and Pd/Al_2O_3(800)-800. According to the HRTEM data (Fig. 7), this is related to the aggregation and sintering of the PdO particles, which is reflected in the decrease of the catalytic efficiency (Fig. 10).

Finally, let us present the XPS data for the sample Pd/Al_2O_3(800)-1200, where palladium existed in the form of large metal particles after calcination at 1200 °C. Treatment with the reaction mixture resulted in a substantial broadening of the Pd3d line, with a slight shift to lower binding energies (Fig. 13e and e′). Curve fitting analysis showed the decomposition of the experimental Pd3d line on two doublets with $E_b(3d_{5/2}) = 335.1$ and 336.7 eV. These doublets can undoubtedly be attributed to metallic and oxide palladium particles. It is noteworthy that the Pd3d line intensity increased by 3 times in comparison with the same value for the initially calcined sample. These data give reliable evidence about the dispergation process during the reaction. The process of dispergation is accompanied by oxidation of some part of the metallic particles in the PdO form.

4. Discussion

The obtained results show that platinum or palladium deposition on γ-Al_2O_3 calcined at different temperatures does not alter its structure. The supported noble metals exist in two states: as clusters (1–3 nm) and aggregates (20–100 nm). According to the HRTEM and XPS data, there are two states of platinum in the Pt/Al_2O_3(550)-450 catalyst both before and after reaction—Pt^0 and PtO_x. No strong interaction between platinum and the support was observed at this calcination temperature. Such behavior of platinum can be explained by a high ratio between the bond strengths in the metal and oxidized platinum E(Pt–Pt)/E(Pt–O) and weak interactions with the support. Under otherwise similar conditions, this results in the formation of three-dimensional metal nanoparticles.

In contrast to platinum, palladium showed a much greater variety of forms after its deposition on the γ-Al_2O_3 surface, which is due to stronger interaction with the support and higher oxygen affinity. The support and catalyst calcination temperatures and the action of the reaction mixture are important factors accounting for this variety.

4.1. Effect of the support calcination temperature on the forms and state of palladium

Palladium on the surface of γ-Al_2O_3 calcined at low temperature (550 °C) in the Pd/Al_2O_3(550)-450 catalyst was in a strongly bound state due to the strong metal–support interaction that was morphologically observed as the decoration effect. This was confirmed by the following data. First, the oxidized palladium nanostructures were not reduced with hydrogen in the temperature range of −15 to 450 °C. Second, increased binding energies were observed in the XPS spectra for both the low-energy component (336.1 eV) and the high-energy one (338.1 eV). The low-energy component corresponded to palladium clusters, whereas the high-energy one was attributed to palladium introduced into the alumina lattice as surface aluminate. Third, the UV–vis DRS data proved that Pd^{2+} ions were present in the palladium–aluminate clusters on the surface of the decorated palladium metal particles. Fourth, according to the HRTEM data, the metal clusters interact epitaxially with the support. The surface of the metal particles is almost completely covered by a thin layer of the support, i.e., by islands of the aluminate phase layers.

Thus, the observed strong interaction of palladium with the surface of the Al_2O_3 support calcined at relatively low temperatures (∼550 °C) is related to the formation of clusters of the aluminate (ionic state of palladium) and metal phases. The metal clusters are stabilized due to the formation of epitaxial bonds between the palladium clusters and the sections of the support surface ordered in the [1 1 1] direction. Conversely, the stabilization of the surface aluminate phase clusters is more likely on extended surface defects or on the surface of the metal clusters. Thus, the observation of the two palladium phase states is directly related to the decoration effect where the palladium metal clusters are covered with a thin layer of the support in the form of the palladium–aluminate phase. It is noteworthy that effects of Pd stabilization on alumina shift the thermodynamic equilibrium to side of Pd^0 particles formation, so we could observe some part of palladium particles in metallic state even after calcinations in O_2 ambient.

Calcination of the support at low temperatures appeared to play a key role. Apparently, support calcination at 550 °C did not completely structure either the bulk or the surface of the γ-Al_2O_3. Indeed, the XRD data (Fig. 1) indicated that the lines of the oxide calcined at 550 °C were poorly resolved. After treatment at a higher temperature (800 °C), their intensity grew and the lines became well resolved. Therefore, it is clear that the high degree of disordering on the γ-Al_2O_3 surface facilitates the formation of chemical bonds and rearrangement of the surface, leading to the formation of more stable compounds and clusters during its interaction with the palladium salts and the following calcination.

An increase of the support calcination temperature to 800 °C significantly changed the palladium interaction with the γ-Al_2O_3 surface. In this case, two forms of palladium were observed by XPS on the surface of the Pd/Al_2O_3(800)-450,

Pd/Al_2O_3(800)-600 and Pd/Al_2O_3(800)-800 catalysts, corresponding to the oxidized $\{E_b(Pd3d_{5/2}) \sim 336.8–337.3\,eV\}$ and reduced $\{E_b(Pd3d_{5/2}) \sim 335.1–335.4\,eV\}$ palladium states. The HRTEM and UV–vis DRS results showed that individual particles interacting with the support and aggregated particles not interacting with the support were present on the surface of Al_2O_3 calcined at 800 °C. The small palladium particles in these samples were epitaxially bound to the surface of the [1 1 1] Al_2O_3 face. The predominant fraction of the metal surface was covered with an Al_2O_3 layer, most likely in the form of the aluminate phase. A substantial part of palladium in these particles was oxidized in the form of PdO from the side of contact with the Al_2O_3 surface with the shift from the initial surface to form core–shell structures. There were some surfaces of the metal particles that were not covered with the aluminum oxide layer. These are the aggregates of the reduced and oxidized states of palladium in various morphological forms that generate the integral photoelectron spectrum of the Pd3d line. In particular, the sum of the components corresponding to PdO and the aluminate layers gives a line with E_b varying in the range of 336.8–338 eV, depending on the relative contribution of the components. Thus, the observed shift of the oxidized components to larger E_b after the treatment of the catalysts (Fig. 12) indicated changes in the relative contributions of PdO and the aluminate phase.

Thus, the decoration effect typical for the catalysts prepared using the support calcined at 550 °C was also observed for the catalysts synthesized with the support calcined at 800 °C. However, in the latter case, three-dimensional nanoparticles rather than flat palladium metal clusters were formed and the decoration degree was lower. Additionally, some palladium metal was converted to PdO nanoparticles, and their fraction grew.

A further increase of the calcination temperature of the Pd/Al_2O_3 catalyst to 1000 °C resulted in the growth and ordering of the palladium metal and, particularly, oxide particles not interacting with the support and existing in the agglomerated form. However, there were still Pd^0 particles on the surface of the support that were stabilized on the alumina surface in a nanosized state due to decoration with the support, which was proven by the HRTEM, UV–vis DRS and XPS data.

Calcination of the Pd/Al_2O_3 catalyst at 1200 °C lead to a reduction of the large agglomerated PdO to Pd^0 particles, which is in agreement with the data obtained by physicochemical methods. The formation of large palladium metal particles is reflected in the XPS spectra as an increase of the binding energy $E_b(Pd3d_{5/2})$ to 336.2 eV due to the charging and final state effects [63–65]. The support is converted after high-temperature calcination to the α-Al_2O_3 phase in the form of large particles.

4.2. Effect of the reaction mixture on the forms and states of palladium

The observed differences in the states and morphology of supported noble metals in $Pt(Pd)/Al_2O_3$ catalysts also affected their performances in CO oxidation. The reaction mixture, in turn, actively affects the state and morphology of the active component.

CO oxidation on palladium metal is known to follow the Langmuir–Hinshelwood mechanism. The light-off temperature within this mechanism is largely determined by the CO adsorption energy [66–70]. According to the literature data, the energies of CO adsorption on clean metal surfaces are 126–134 kJ/mol for Pt [71] and 142–167 kJ/mol for Pd [72]. The energies of CO adsorption in the linear and bridging forms are 220 and 94 kJ/mol for Pt/Al_2O_3 catalysts [73,74] and 92 and 168 kJ/mol for Pd/Al_2O_3 catalysts [75]. Based on these data, one can assume that the lower efficiency of the Pt/Al_2O_3(550)-450 catalyst compared to the Pd/Al_2O_3(550)-450 catalyst is largely determined by the higher CO adsorption energy.

The efficiency of the palladium catalysts in the CO oxidation depends on the support calcination temperature. T_{50} was equal to 150 and 145 °C for the Pd/Al_2O_3(550)-450 and Pd/Al_2O_3(800)-450 catalysts, respectively. Therefore, the increase of the support calcination temperature from 550 to 800 °C made the catalyst more active (for the catalysts calcined at the same temperature (450 °C)), although the CO conversion increase was not very large. This CO conversion increase may be either due to the decreased size of the palladium particles or the change of their interaction with the support. The latter effect is supported by the decrease of the reduction temperature in the TPR-H_2 spectra and decrease of $E_b(Pd3d_{5/2})$ of the high-energy component in the Pd3d spectra from 338.1 to 336.8 eV. The weakening of the interaction with the support is also reflected in the growth of the metal state fraction and decrease of the oxide fraction in the Pd/Al_2O_3(800)-450 catalyst after reaction with $CO + O_2$, whereas the state of palladium in the Pd/Al_2O_3(550)-450 was not changed. Thus, palladium in the Pd/Al_2O_3(800)-450 catalyst was reduced more easily under by the reaction mixture. The weakening of the Pd interaction with Al_2O_3 makes the catalyst more active. Note that the CO conversion of the Pd/Al_2O_3(800) catalysts goes down when their calcination temperature is increased from 450 to 800 °C. Apparently, this is related to the loss of some small palladium metal particles decorated with the support due to sintering with partial conversion to PdO agglomerates. Meanwhile, the activity of the PdO agglomerates was lower than that of oxygen adsorbed on the surface of palladium metal [76].

The fastest loss of activity was observed when the catalyst calcination temperature was increased to 1000 and 1200 °C going from Pd/Al_2O_3(800)-800 to Pd/Al_2O_3(800)-1000 and Pd/Al_2O_3(800)-1200 catalysts. In this case, T_{50} grew from 145 to 189 °C. This was due to a substantial growth of the Pd particles from 2 to 3 nm (individual particles) and 20 nm (agglomerates) to 3–7 and 100 nm, respectively, and a significant decrease of the number of small particles. As noted above, the fraction of the PdO particle agglomerates was high in the sample calcined at 1000 °C. After calcination at 1200 °C, they were transformed into large metal particles. The energy of the CO adsorption on large metal particles should be close to that on bulk palladium. This change leads to a increase of the light-off temperature and shift of the CO conversion curve to high temperatures.

Note that the reaction mixture substantially affects the active component morphology. For example, treatment of the Pd/Al_2O_3(800)-1000 catalyst with the reaction mixture is accompanied by the palladium redox processes, resulting in palladium dispersion to form small metal particles.

5. Conclusions

The noble metal (Pd, Pt) particles on γ-Al_2O_3 were studied by a variety of physicochemical methods, including XRD, UV–vis DRS, HRTEM, TPR-H_2, XPS, and catalytic properties measurements. We performed systematic study of $Pd(Pt)/\gamma$-Al_2O_3 catalysts depending on the calcination temperature of the support/catalyst and the $CO + O_2$ treatment. It was established that for all studied samples of $Pd(Pt)/\gamma$-Al_2O_3 catalysts, the particles of the active component are randomly distributed on the surface of Al_2O_3 and correspond to single particles with sizes of 1.5–3 nm, as well as agglomerates $\sim$ 100 nm. In the Pt/Al_2O_3(550)-450 catalyst, the small particles corresponded to individual metallic clusters on the support surface. However, in the Pd/Al_2O_3(550)-450 catalyst, the palladium particles were almost completely decorated with a thin layer of an aluminate phase. The formation of epitaxial bonding between Pd^0 metallic clusters and the Al_2O_3(1 1 1) surface of support was also clear. These structures are not reduced in hydrogen in the temperature range of −15 to 450 °C and are stable to treatment with a mixture of $CO + O_2$.

Investigation of the $Pd/Al_2O_3(800)$-*T* catalysts revealed the formation of decorated metallic particles with a core-shell structure. A metallic core of this structure was covered by a palladium–aluminate phase as in the case of the $Pd/Al_2O_3(550)$-450 catalyst. It was established that these core-shell structures localized on the γ-Al_2O_3 surface are extremely stable under the reaction mixture.

Depending on the calcination temperature of the catalyst in the range of 450–1000 °C, the morphological form of the active component was converted from the "core-shell" state to the state consisting of two phases, Pd^o and PdO, with a gradual decrease of the Pd^o/PdO ratio, weakening the interaction with the support and the growth of the palladium particles. This process is accompanied by enlargement of PdO agglomerates, while small Pd^o particles remain in a nanosized state as a consequence of its decoration by the support. Calcination of the Pd/Al_2O_3 catalyst at 1200 °C promoted the reduction of coarse PdO particles into Pd^o. Under the action of the reaction mixture, the catalysts $Pd/Al_2O_3(800)$-(450,600,800,1000) were able to change their Pd^o/PdO ratio, which regulates the light-off temperature. After the catalyst calcination at the highest temperature used in this study (1200 °C), the palladium particles became much larger due to the loss of interaction with the support. Only the metal phase of palladium was observed in these catalysts, and their catalytic performance was very poor.

References

[1] R.K. Oberlander, Appl. Catal. 3 (1984) 64.
[2] C. Morterra, G. Magnacca, Catal. Today 27 (1996) 497.
[3] C.-B. Wang, H.-G. Lee, T.-F. Yeh, S.-N. Hsu, K.-S. Chu, Thermochim. Acta 401 (2003) 209.
[4] T. Ishihara, K. Harada, K. Eguchi, H. Arai, J. Catal. 136 (1992) 161.
[5] A.Y. Stakheev, L.M. Kustov, Appl. Catal. A 188 (1999) 3.
[6] S.-D. Mo, Y.-N. Xu, W.-Y. Ching, J. Am. Ceram. Soc. 80 (1997) 1193.
[7] D. Ciuparu, L. Pfefferle, Appl. Catal. A-Gen. 209 (2001) 415.
[8] N.M. Rodriguez, S.G. Oh, R.A. DallaBetta, R.T.K. Baker, J. Catal. 157 (1995) 676.
[9] K. Otto, L.P. Haack, J.E. deVries, Appl. Catal. B-Environ. 1 (1992) 1.
[10] K. Otto, C.P. Hubbard, W.H. Weber, G.W. Graham, Appl. Catal. B-Environ. 1 (1992) 317.
[11] J. Goetz, M.A. Volpe, A.M. Sica, C.E. Gigola, R. Touroude, J. Catal. 153 (1995) 86.
[12] V.H. Sandoval, C.E. Gigola, Appl. Catal. A-Gen. 148 (1996) 81.
[13] H.C. Yao, M. Sleg, H.K. Phunmer Jr., J. Catal. 59 (1979) 365.
[14] Farrauto S.J., J.K. Lampert, M.C. Hobson, E.M. Waterman, Appl. Catal. B-Gen. 6 (1995) 263.
[15] A.K. Datye, J. Bravo, T.R. Nelson, P. Atanasova, M. Lyubovsky, L. Pfefferle, Appl. Catal. A-Gen. 198 (2000) 179.
[16] T.E. Hoost, K. Otto, Appl. Catal. A-Gen. 92 (1992) 39.
[17] E. Lesage-Rosenberg, G. Vlaic, H. Dexpert, P. Lagarde, E. Freund, Appl. Catal. 22 (1986) 211.
[18] S. Damyanova, J.M.C. Bueno, Appl. Catal. A: Gen. 253 (2003) 135.
[19] P.O. Graf, D.J.M. de Vlieger, B.L. Mojet, L. Lefferts, J. Catal. 262 (2009) 181.
[20] D. Roth, P. Gelin, M. Primet, E. Tena, Appl. Catal. A: Gen. 203 (2000) 37.
[21] H. Yoshida, T. Nakajima, Y. Yazawa, T. Hattori, Appl. Catal. B: Environ. 71 (2007) 70.
[22] Lieske, J. Voelter, J. Phys. Chem. 89 (1985) 1841.
[23] J.J. Chen, E. Ruckenstein, J. Phys. Chem. 85 (1981) 1606.
[24] T. Lear, N.G. Hamilton, D. Lennon, Catal. Today 126 (2007) 219.
[25] A. Martínez-Arias, A.B. Hungría, M. Fernández-García, A. Iglesias-Juez, J.A. Anderson, J.C. Conesa, J. Catal. 221 (2004) 85–92.
[26] K. Arnby, A. Törncrona, B. Andersson, M. Skoglundh, J. Catal. 221 (2004) 252.
[27] A. Kubacka, et al., J. Catal. (2010), doi:10.1016/j.jcat.2010.01.008.
[28] A. Bourane, D. Bianchi, J. Catal. 202 (2001) 34.
[29] J.E. Turner, B.C. Sales, M.B. Maple, Surf. Sci. 109 (1981) 591.
[30] W.J. Price, Analytical atomic-absorption spectroscopy, Heyden & Son Ltd, London-New York-Rheine, 1972.
[31] H.-P. Boehm, H. Knozinger, in: J.R. Anderson, M. Boudart (Eds.), Catalysis Science and Technology, vol. 4, Springer-Verlag, Berlin/Heidelberg/New York, 1983, pp. 39–209.
[32] E.M. Slavinskaya, Yu.A. Chesalov, A.I. Boronin, I.A. Polukhina, A.S. Noskov, Kinet. Catal. 46 (2005) 555.
[33] A.I. Titkov, A.N. Salanov, S.V. Koscheev, A.I. Boronin, React. Kinet. Catal. Lett. 86 (2005) 371.
[34] A.S. Knyazev, O.V. Magaev, O.V. Vodyankina, A.I. Titkov, A.N. Salanov, S.V. Koshcheev, A.I. Boronin, Kinet. Catal. 46 (2005) 151.
[35] J.F. Moulder, W.F. Stickle, P.E. Sobol (Eds.), Handbook of X-ray Photoelectron Spectroscopy, Perkin-Elmer Corporation, Physical Electronics Division, Eden Prairie, MN, 1992.
[36] S. Lowell, J.E. Shields, M.A. Thomas, M. Thommes, Characterization of Porous Solids and Powders: Surface Area, Pore Size and Density, Springer, Netherlands, 2006.
[37] A.B.P. Lever, Inorganic Electronic Spectroscopy, vol. 2, Elsevier, Amsterdam/Oxford/New York/Tokyo, 1984, p. 491.
[38] L.I. Elding, L.F. Olsson, J. Phys. Chem. 82 (1978) 69.
[39] R.P. Messmer, U. Wahlgen, K.H. Johnson, Chem. Phys. Lett. 18 (1973) 7.
[40] A. Rakai, D. Tessier, F. Bozon-Verduraz, New J. Chem. 16 (1992) 869.
[41] A.B. Gaspar, L.C. Diegues, Appl. Catal. A: Gen. 201 (2000) 241.
[42] D.A.M. Monti, A. Baiker, J. Catal. 83 (1983) 323.
[43] S. Komhoma, O. Mekasuwandumrong, P. Praserthdam, J. Panpranot, Catal. Commun. 10 (2008) 86.
[44] E.A. Sales, J. Jove, M. de Jesus Mendes, F. Bozon-Verduraz, J. Catal. 195 (2000) 88.
[45] M. Delage, B. Didillon, Y. Huiban, J. Lynch, D. Uzio, Stud. Surf. Sci. Catal. 130 (2000) 1019.
[46] R.J.H. Grisel, J.J. Slyconish, B.E. Niewenhuys, Top. Catal. 16/17 (2001) 425.
[47] A. Bourane, D. Bianchi, J. Catal. 209 (2002) 114.
[48] D.A. Shirley, Phys. Rev. B 5 (1972) 4709.
[49] Grisel Corro, J.L.G. Fierro, Vazquez C. Odilon, Catal. Commun. 4 (2003) 371.
[50] J.C. Serrano-Ruiz, G.W. Huber, M.A. Sánchez-Castillo, J.A. Dumesic, F. Rodríguez-Reinoso, A. Sepúlveda-Escribano, J. Catal. 241 (2006) 378.
[51] J.Z. Shyu, K. Otto, Appl. Surf. Sci. 32 (1998) 246.
[52] R. Bouwman, P. Biloen, J. Catal. 48 (1977) 209.
[53] M. Brun, A. Berthet, J.C. Bertolini, J. Electron Spectrosc. Relat. Phenom. 104 (1999) 55.
[54] D. Briggs, M.P. Seah, Practical Surface Analysis, vol. 1, second ed., Wiley, Chichester, 1990.
[55] S. Suhonen, M. Valden, M. Pessa, A. Savimaki, M. Harkonen, M. Hietikko, J. Pursiainen, R. Laitinen, Appl. Catal. 207 (2001) 113.
[56] C.E. Gigola, M.S. Moreno, I. Costilla, M.D. Sanchez, Appl. Surf. Sci. 254 (2007) 325.
[57] V.A. dela Pena, O. Shea, M.C. Alvarez-Galvan, J. Requies, V.L. Barrio, P.L. Arias, J.F. Cambra, J.L.G. Fierro, Catal. Commun. 8 (2007) 1287.
[58] L.S.F. Feio, C.E. Hori, S. Damyanova, F.B. Noronha, W.H. Cassinelli, C.M.P. Marques, J.M.C. Bueno, Appl. Catal. A: Gen. 316 (2007) 107.
[59] D. Gao, C. Zhang, Sh. Wang, Z. Yuan, S. Wang, Catal. Commun. 9 (2008) 2583.
[60] B. Mirkelamoglu, G. Karakas, Appl. Catal. A: Gen. 299 (2006) 84.
[61] M.R. Mucalo, R.P. Cooney, J.B. Metson, Colloids Surf. 60 (1991) 175.
[62] L.S. Kibis, A.I. Titkov, A.I. Stadnichenko, S.V. Koscheev, A.I. Boronin, Appl. Surf. Sci. 255 (2009) 9248.
[63] Z. Bastl, Vacuum 36 (1985) 447.
[64] G.K. Wertheim, Z. Phys. B. Condens. Matter 66 (1987) 53.
[65] A.I. Boronin, Condens. Matter Interfaces 2 (2000) 4, in Russian.
[66] G. Ertl, Oscillatory catalytic reactions at single-crystal surfaces, Adv. Catal. 37 (1990) 213.
[67] M. Bowker, I.Z. Jones, R.A. Bennett, F. Esch, A. Baraldi, S. Lizzit, G. Comelli, Catal. Lett. 51 (1998) 187.
[68] I. Jones, R. Bennett, M. Bowker, Surf. Sci. 439 (1999) 235.
[69] A. Bourane, D. Bianchi, J. Catal. 209 (2002) 126.
[70] A. Bourane, D. Bianchi, J. Catal. 222 (2004) 499.
[71] W.H. Weinberg, C.M. Comrie, R.M. Lambert, J. Catal. 41 (1976) 489.
[72] H. Conrad, G. Ertl, J. Koch, E.E. Latta, Surf. Sci. 43 (1974) 462.
[73] A. Bourane, D. Bianchi, J. Catal. 218 (2003) 447.
[74] P. Pillonel, S. Derrouiche, A. Bourane, F. Gaillard, P. Vernoux, D. Bianchi, Appl. Catal. A: Gen. 278 (2005) 223.
[75] O. Dulaurent, R. Chandes, C. Bouly, D. Bianchi, J. Catal. 188 (1999) 237.
[76] T. Schalow, B. Brandt, M. Laurin, S. Schauermann, J. Libuda, H.-J. Freund, J. Catal. 242 (2006) 58.